

Probing ultra-diffuse galaxies out to the virial radius of the Coma cluster with *XMM–Newton*

M. S. Mirakhor^{*} and S. A. Walker

Department of Physics and Astronomy, The University of Alabama in Huntsville, Huntsville, AL 35899, USA

Accepted XXX. Received YYY; in original form ZZZ

ABSTRACT

We probe the formation scenarios and AGN occupation fraction of ultra-diffuse galaxies (UDGs) in the nearby Coma cluster by utilizing *XMM–Newton* observations of 779 out of 854 UDG candidates identified by Subaru survey. Their origin is probed by measuring the dark matter halo mass of the stacked sample of UDGs and the population of low-mass X-ray binaries residing in globular clusters. Our measurements suggest that the average UDG population does not have a substantial amount of hot gas or a large number of globular clusters. This supports the formation scenario, in which UDGs are puffed-up dwarf galaxies, agreeing with that obtained for 404 Coma cluster UDGs using *Chandra*. We also determine the active galactic nuclei (AGN) occupation fraction of UDGs by cross-correlating the position of UDGs with the detected point sources in Coma. We detect three X-ray sources with detection significance $\sigma \geq 5$ that could be off-centre AGN within 5 arcsec from the centre of the UDG 317, UDG 432, and UDG 535. We identify an optical counterpart for the X-ray source associated with the UDG 317, suggesting that this source is more likely an off-centre AGN. Based on the current data, however, we cannot conclusively constrain whether the detected AGN is residing in the Coma cluster or not.

Key words: galaxies: clusters: individual (Coma) – X-rays: general – X-rays: galaxies – galaxies: formation

1 INTRODUCTION

The presence of large, extremely faint systems in galaxy clusters is not a recent discovery (e.g. [Impey et al. 1988](#)). However, deep imaging surveys of nearby galaxy clusters (e.g. [Mihos et al. 2015](#); [Muñoz et al. 2015](#)) have only recently revealed a copious population of faint systems that has remained relatively unexplored in shallower surveys. Perhaps the most interesting result is the discovery of a large population of massive but extremely faint galaxies in the Coma cluster ([van Dokkum et al. 2015](#)), using the Dragonfly Telephoto Array ([Abraham & van Dokkum 2014](#)). These galaxies, which were dubbed as ultra-diffuse galaxies or UDGs, have very low central surface brightness ($\mu_{g,0} \gtrsim 24$ mag arcsec⁻²) with large effective radii ($r_{\text{eff}} > 1.5$ kpc) similar to Milky Way-type galaxies.

While their existence is well established, it is still an open question of how UDGs fit into the general picture of galaxy formation and evolution. Despite the abundance of UDGs in galaxy clusters, their formation and evolutionary pathways can be constrained to two main formation scenarios ([Kovács et al. 2019](#)). The first scenario is that UDGs are "failed" massive galaxies that were prevented from further star formation by gas removal (e.g. [van Dokkum et al. 2015, 2016](#)). The second one is that they are genuine dwarf galaxies, and their large spatial extent is caused by strong feedback from supernovae or active galactic nuclei (AGN) activity (e.g. [Beasley et al. 2016](#); [Amorisco & Loeb 2016](#); [Peng & Lim 2016](#)). The former scenario suggests that UDGs reside in massive dark matter halos, while in the second scenario, UDGs are expected to reside in low-mass dark matter halos.

This difference implies that one can constrain the formation scenarios of UDGs by measuring their dark matter halo mass.

X-ray observations provide a powerful tool to probe the total mass distribution in galaxies. Several studies (e.g. [Babyk et al. 2018](#); [Lakhchaura et al. 2018](#)) found that the X-ray luminosity is proportional to the total gravitating mass of galaxies. Therefore, massive galaxies are expected to have higher X-ray luminosities than low-mass galaxies. [Kovács et al. \(2019\)](#) employed *XMM–Newton* observations to probe the formation scenarios for a sample of isolated UDGs by constraining their dark matter halos. No statistically significant emission from the individual UDGs or from the stacked sample of UDGs was detected. The absence of significant emission implies the lack of a massive dark matter halo. This, in turn, suggests that the bulk of isolated UDGs reside in low-mass dark matter halos.

More recently, [Kovács et al. \(2020\)](#) probed the formation scenarios for a sample of UDGs residing in the nearby Coma cluster, using a similar analysis to that done in [Kovács et al. \(2019\)](#). Specifically, they carried out a *Chandra* X-ray analysis on 404 out of 854 UDGs detected within the field of Coma by the Subaru Suprime-Cam survey ([Yagi et al. 2016](#)). The formation scenarios of UDGs were probed by measuring the X-ray luminosity of the hot diffuse gas around UDGs and low-mass X-ray binaries (LMXBs) residing in globular clusters (GCs). They also did not detect significant X-ray emission from the hot gas or from GC-LMXBs. Based on the upper limits on the X-ray luminosity, [Kovács et al. \(2020\)](#) concluded that the bulk of the UDG population in the Coma cluster are genuine dwarf galaxies. This conclusion resonates well with that derived for isolated UDGs ([Kovács et al. 2019](#)).

Moreover, [Kovács et al. \(2020\)](#) constrained the occupation fraction

^{*} E-mail: msm0033@uah.edu

of AGN in UDGs by cross-correlating the position of UDGs with the identified X-ray sources in the Coma cluster. They only identified two UDGs that have off-centre source, which might be AGN, at distances of 3.0 and 3.2 arcsec from the centre of the UDG 317 and UDG 412. This implies an AGN occupation fraction of about 0.5 per cent, which is comparable to that found for low-mass galaxies.

However, the reported results in the work of Kovács et al. (2020) are based on 404 UDGs, which only represents around 47 per cent of the full list of UDG candidates detected in the Coma cluster. In this work, taking advantage of our high-quality *XMM-Newton* data of the Coma cluster that cover the cluster out to the virial radius (Mirakhor & Walker 2020a), we rely on a larger sample of UDGs to probe their formation scenarios and AGN occupation fraction. As our data cover a larger region of Coma, we have *XMM-Newton* observations for 779 out of 854 UDG candidates in the Coma cluster, excluding the central 4 arcmin region. This number is almost twice the number of UDGs (404 UDGs) studied in Kovács et al. (2020), and represents around 91 per cent of UDG candidates identified in the Coma cluster. This large sample of UDGs would provide a better constraint on their origin and AGN occupation fraction.

The X-ray analysis adopted in the current work is essentially the same as the one by Kovács et al. (2020), but we now apply this analysis on 779 UDGs instead of 404 UDGs. As in Kovács et al. (2020), we also rely on the publicly-available data for 854 UDG candidates in the Coma cluster (Yagi et al. 2016). The spatial distribution of these UDGs cover a region of $1.7 \times 2.7 \text{ deg}^2$ of the Coma cluster. As spectroscopic measurements are not available for a large fraction of them, we cannot conclusively determine whether these galaxies are members of the Coma cluster. However, based on the radial velocity measurements of sub-samples of UDG candidates, several studies (e.g. van Dokkum et al. 2016, 2017) found that the vast majority of UDG candidates reside in the Coma cluster. We, therefore, consider that all UDG candidates reside in the Coma cluster, as is done in Kovács et al. (2020).

Throughout this work, we adopt a Λ cold dark matter cosmology with $\Omega_m = 0.3$, $\Omega_\Lambda = 0.7$, and $H_0 = 100 h_{100} \text{ km s}^{-1} \text{ Mpc}^{-1}$ with $h_{100} = 0.7$. At the redshift of Coma, 1 arcsec corresponds to 0.48 kpc. Uncertainties are at the 68 per cent confidence level, unless otherwise stated.

2 OBSERVATIONS AND DATA REDUCTION

In this work, we used 61 *XMM-Newton* observations in the field of the Coma cluster that cover the cluster out to the virial radius with nearly complete azimuthal coverage. These observations were taken in the period between 2000 and 2019, and the total observation duration is around 2.3 Ms. The details of all *XMM-Newton* observations used in this work are summarized in Table A1.

We reduced the X-ray data using *XMM-Newton* Science Analysis System (XMM-SAS) version 18.0 and Current Calibration Files (CCF), following the methods described in the Extended Source Analysis Software (ESAS) cookbook¹, as is also done in Mirakhor & Walker (2020a,b). We initiated the data processing by running the *epchain* and *emchain* scripts, followed by the ESAS tasks *mos-filter* and *pn-filter* to filter the data for soft-proton flares and produce event files for MOS and PN detectors. We screened the data in the MOS detectors for CCDs in anomalous states, and any affected CCDs were then excluded from further analysis. The ESAS source-detection tool

cheese was used to detect point sources and extended substructures. The next step in data processing is to create spectra, RMFs, ARFs, event images, and exposure maps for the entire region of interest using the *mos-spectra* and *pn-spectra* tasks. Then, by running the *mos-back* and *pn-back* tasks, the intermediate files created by *mos-spectra* and *pn-spectra* were turned into the quiescent particle background spectra and images in detector coordinates.

We further examined the data for residual soft-proton contamination that may have remained after light-curve filtering. After the spectral parameters for the soft-proton contamination have been derived, the *proton* task was run to produce images of the soft proton contamination in detector coordinates. We also applied an additional screening step by running the *Chandra* tool *wavdetect* to detect point sources and extended substructures within the field of view that were missed using the ESAS tool *cheese*.

After weighting the MOS and PN detectors for all of the *XMM-Newton* observations by their relative effective area, the main components for a background-subtracted and exposure-corrected image produced from the analysis procedure described above were then merged and adaptively smoothed into a single image. Following Kovács et al. (2020), we created X-ray images in the soft (0.5–1.2 keV) and broad (0.5–7.0 keV) bands to account for the X-ray emission from hot gaseous halos and LMXBs, respectively. These energy bands were chosen to maximize the signal-to-noise ratio of the detection of the hot gas and the population of LMXBs.

For the soft-energy band, an optically-thin plasma emission is assumed, with a temperature of 0.2 keV and an iron abundance of $0.2 Z_\odot$ to describe gaseous emission of UDGs. This assumption is motivated by the observed temperature and iron abundance of spiral and low-mass elliptical galaxies (e.g. Goulding et al. 2016). Although some individual galaxies could have different values for the gas temperature and iron abundance, it is unexpected that this variation affects our results, as we are studying a large number of galaxies. For broad-energy band, we assumed that the LMXB emission follows a power-law spectrum with an index of 1.7 (e.g. Irwin et al. 2003; Piconcelli et al. 2005), as in Kovács et al. (2020).

In Fig. 1, we show the *XMM-Newton* mosaicked image of the Coma cluster in the energy band 0.5–1.2 keV. The small cyan circles ($r = 40$ arcsec) mark the locations of the UDG candidates in the Coma cluster detected in the Subaru survey (Yagi et al. 2016). The white contours show the full extent of the *Chandra* mosaic explored in Kovács et al. (2020). The bulk of the on-axis *Chandra* exposure time (around 1.6 Ms of the 2.0 Ms total) is concentrated in 2 central pointings, shown by the yellow contours. Our complete *XMM-Newton* mosaic, with full coverage of Coma out to the virial radius in all directions, allows us to provide a near complete X-ray survey of the UDGs identified in the Subaru survey. By using a large mosaic of *XMM-Newton* observations of the Coma cluster, we find that 786 UDG candidates have *XMM-Newton* observations.

As in Kovács et al. (2020), we excluded the central 4 arcmin region of the Coma cluster from our analysis since the X-ray emission in this region is mainly dominated by the hot intracluster medium gas that distributed between galaxies (e.g. Mirakhor & Walker 2020a), which is significantly higher than the emission expected from UDGs. Beyond this radius, as the surface brightness of the intracluster medium drops significantly, it is expected the X-ray emission from various components of UDGs to play a more significant role. We find that there are only 7 UDG candidates in the central 4 arcmin region. By excluding these UDGs, the total number of UDGs analysed in this work reduces to 779 UDGs. This number makes about 91 per cent of the full sample of UDGs detected by Subaru survey (Yagi et al. 2016),

¹ <https://heasarc.gsfc.nasa.gov/docs/xmm/esas/cookbook/xmm-esas.html>

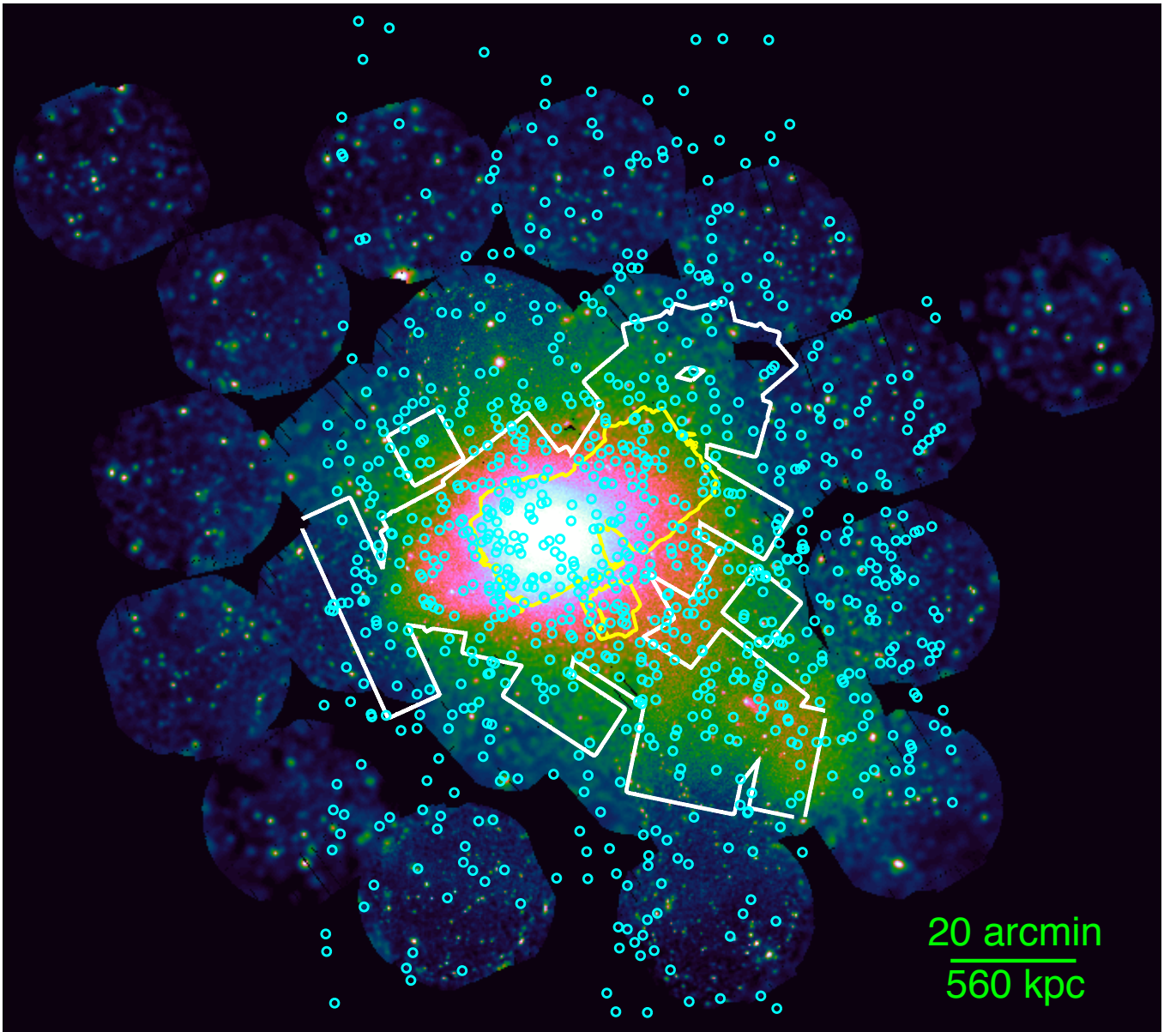


Figure 1. *XMM–Newton* mosaicked image of the Coma cluster in the energy band 0.5–1.2 keV. The small cyan circles are centred on the UDG coordinates as given by Subaru survey (Yagi et al. 2016), and each set to have a radius of 40 arcsec to aid visibility. The white contours show the full extent of the *Chandra* mosaic explored in Kovács et al. (2020). The bulk of the on-axis *Chandra* exposure time is concentrated in 2 central pointings, shown by the yellow contours. By excluding the central 4 arcmin region, the *XMM–Newton* observations are available for 779 out of 854 UDG candidates identified in the Coma cluster.

and is almost twice the number of UDGs (404 UDGs) analysed in Kovács et al. (2020) using *Chandra* observations.

3 X-RAY ANALYSIS AND RESULTS

We probe the formation scenarios of UDGs in the Coma cluster using two approaches. In addition, we investigate the AGN occupation fraction of UDGs in the Coma cluster. As discussed in Section 1, we carry out a similar analysis to that described in Kovács et al. (2020), but, in the current work, the X-ray analysis is performed on 779 UDG candidates. Below, we present the approaches that used to probe the formation scenarios and AGN occupation fraction in

the Coma cluster, and the results derived from the *XMM–Newton* analysis.

3.1 Dark matter halo mass

We first probed the formation scenarios of UDGs by measuring the X-ray luminosity of their hot halos in the soft energy band. As the X-ray luminosity of the gaseous X-ray halos is a robust tracer of the total gravitating mass of galaxies (e.g. Kim & Fabbiano 2013; Babyk et al. 2018; Lakhchaura et al. 2018), measuring the X-ray luminosity of the UDG hot halos allows to set a proper constraint on the dark matter halo mass of UDGs, and therefore their formation mechanism. UDGs could be the descendants of massive galaxies if they reside

in massive dark matter halos similar to halos of Milky Way-type galaxies. Alternatively, UDGs could be genuine dwarf galaxies with large spatial extent if they reside in low-mass dark matter halos.

To test whether UDGs reside in massive or low-mass dark matter halos, Kovács et al. (2020) estimated the expected luminosity of the gaseous X-ray halo around a UDG, assuming that it resides in a Milky Way-type dark matter halo with a virial mass of $M_{\text{vir}} = 8.0 \times 10^{11} M_{\odot}$. Within a radius of $5r_{\text{eff}}$, this virial mass corresponds to a total mass of $M_{\text{tot}} = 1.8 \times 10^{11} M_{\odot}$. Using the $L_{0.3-8\text{keV}} - M_{\text{tot}}$ scaling relation (Kim & Fabbiano 2013), the expected X-ray luminosity in the 0.3–8.0 keV band estimated by these authors is $\approx 1.8 \times 10^{39} \text{ erg s}^{-1}$. Assuming a temperature of 0.2 keV and an iron abundance of $0.2 Z_{\odot}$, the corresponding value for the expected luminosity in the 0.5–1.2 keV band is $\approx 1.1 \times 10^{39} \text{ erg s}^{-1}$. This value is relatively small and falls well below the X-ray luminosity of most individual galaxies detected by *XMM-Newton*. To overcome this limitation, Kovács et al. (2020) stacked the X-ray emission originating from individual galaxies, allowing to probe the emission of the average UDG population with better sensitivity.

Following Kovács et al. (2020), we performed the stacking analysis in the soft band (0.5–1.2 keV) to measure the gaseous X-ray luminosity of the UDG population. For each UDG in our sample, we extracted a region of $150 \text{ arcsec} \times 150 \text{ arcsec}$ from the X-ray image and exposure map, centred on the UDG position as given by Subaru survey. We then combined the extracted images and exposure maps for the full list of UDGs in our sample into a single image. Fig. 2 shows the stacked exposure-corrected image of the analysed UDGs in the soft band. Kovács et al. (2020) measured the X-ray luminosity associated with the UDG population within a circular region of 5 arcsec radius. However, as *XMM-Newton* has a broader PSF than *Chandra*, the X-ray counts associated with the UDGs may be scattered to a much larger region. Within a circular region of 5 arcsec radius, only 35 per cent of the PSF is encircled within this region. We therefore considered a larger extraction region for measuring the X-ray luminosity. Motivated by the PSF size of *XMM-Newton*, we extracted the source counts using a circular region of 15 arcsec radius, as we find that 90 per cent of the PSF is enclosed within this region. The background counts were extracted from an annulus region with 25–30 arcsec radii.

After accounting for the stacked source and background counts, we did not obtain statistically significant X-ray emission from the hot halo of the analysed UDGs, agreeing with that reported in Kovács et al. (2020). As a result of the absence of significant X-ray emission, a 2σ upper limit on the X-ray luminosity is computed. Assuming an optically-thin plasma emission with a temperature of 0.2 keV and an iron abundance of $0.2 Z_{\odot}$, we obtain a 2σ upper limit of $< 1.0 \times 10^{-16} \text{ erg s}^{-1} \text{ cm}^{-2}$ on the average X-ray flux of the analysed Coma cluster UDGs in the 0.5–1.2 keV energy range. At the redshift of Coma, this value places a 2σ upper limit of $< 1.2 \times 10^{38} \text{ erg s}^{-1}$ on the X-ray luminosity of the hot gaseous halo. This upper-limit luminosity, although slightly higher than that estimated for the analysed Coma cluster UDGs in Kovács et al. (2020), is about 9 times lower than the luminosity of $1.1 \times 10^{39} \text{ erg s}^{-1}$ estimated for a galaxy with a massive dark matter halo. These results imply that significant fraction of UDGs in the Coma cluster are genuine dwarf galaxies, in good agreement with the results obtained for the Coma cluster UDGs studied in Kovács et al. (2020).

The 2σ upper-limit luminosity of the hot gaseous halo in the soft band corresponds to an X-ray luminosity of $< 2.1 \times 10^{38} \text{ erg s}^{-1}$ in the 0.3–8.0 keV band. Using the best-fitting relation that found between the gas luminosity and total mass (Kim & Fabbiano 2013), this value implies a total mass of $M_{\text{tot}} < 9.0 \times 10^{10} M_{\odot}$ within $5r_{\text{eff}}$. This mass

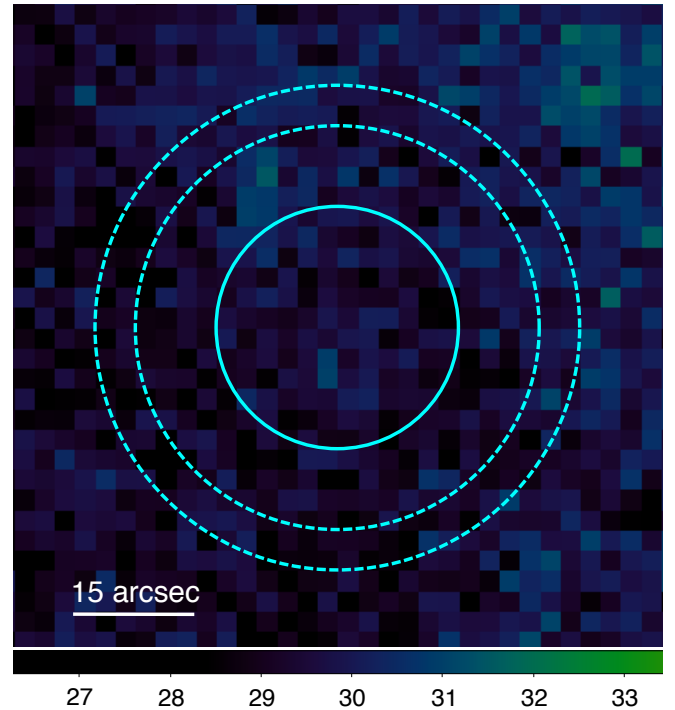


Figure 2. Stacked exposure-corrected image of the analysed Coma cluster UDGs in the soft band. The stacked image centred on the UDG coordinates as given by Subaru survey (Yagi et al. 2016). The cyan circle (solid line) with 15 arcsec radius marks the region where the source counts were extracted. The circular annuli (dashed lines) with radii of 25–30 arcsec marks the region in which the background counts were extracted. We did not obtain significant X-ray emission from the hot halo of the analysed UDGs, suggesting that the bulk of the UDG population in the Coma cluster are genuine dwarf galaxies.

is only half the total mass obtained for a galaxy with a Milky Way-type dark matter halo. In Fig. 3, we show the correlation between the X-ray luminosity of hot gas in the 0.3–8.0 keV band and the total gravitating mass for a sample of early-type galaxies (Kim & Fabbiano 2013), isolated UDGs (Kovács et al. 2019), Coma cluster UDGs (Kovács et al. 2020), and Coma cluster UDGs analysed in this work. In the same figure, we also show the best-fitting relation between the X-ray luminosity and the total gravitating mass obtained from the X-ray scaling relation in early-type galaxies (Kim & Fabbiano 2013).

3.2 GC-LMXB population

We also probe the origin of UDGs in the Coma cluster through their GC-LMXB population, as is done in Kovács et al. (2020). Due to the high-stellar density in the core, GCs can effectively trigger the formation of various types of binaries, including LMXBs (e.g. Kim et al. 2006; Sivakoff et al. 2007). It is well known from X-ray studies (e.g. Sarazin et al. 2000) that the bulk of the X-ray emission in early-type galaxies originates from LMXBs. Also, it is well established that the number of LMXBs per unit stellar mass is a few hundred times higher in GCs than in the galactic field, as stellar densities in the field are typically very low to form LMXBs (e.g. Angelini et al. 2001; Minniti et al. 2004; Jordán et al. 2007). Therefore, we do not expect to see significant amount of the X-ray emission from field LMXBs. On the other hand, if UDGs reside in massive dark matter halos and host large numbers of GCs as found in two Coma cluster UDGs: Dragonfly 44 and DF X1 (van Dokkum et al. 2017),

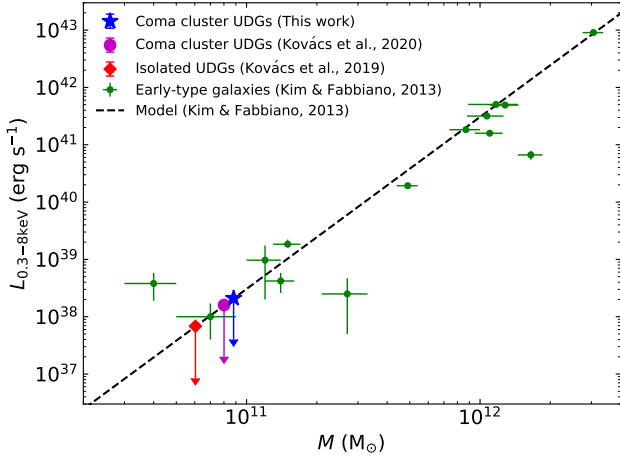


Figure 3. Correlation between the X-ray luminosity of hot gas in the 0.3–8.0 keV band and the total gravitating mass for a sample of early-type galaxies (Kim & Fabbiano 2013), isolated UDGs (Kovács et al. 2019), Coma cluster UDGs (Kovács et al. 2020), and Coma cluster UDGs analysed in this work. Using the best-fitting relation (Kim & Fabbiano 2013), the 2σ upper limit on the X-ray luminosity implies a total mass of $< 9.0 \times 10^{10} M_{\odot}$ within $5r_{\text{eff}}$. Although this mass is slightly higher than a mass of $< 8.0 \times 10^{10} M_{\odot}$ estimated for the analysed Coma cluster UDGs in Kovács et al. (2020), it is only half the total mass obtained for a galaxy with a massive dark matter halo. This suggests that the bulk of UDGs in the Coma cluster reside in low-mass dark matter halos.

significant amount of the X-ray emission is then expected from GC-LMXBs. By comparing the X-ray luminosity of GC-LMXBs with the luminosity expected from a galaxy with a massive dark matter halo, one can constrain whether the bulk of the UDG population hosts a large number of GCs. Consequently, this allows us to determine whether UDGs reside in massive or low-mass dark matter halos.

As discussed in Section 3.1, if we assume that UDGs reside in massive dark matter halos with a virial mass of $M_{\text{vir}} = 8.0 \times 10^{11} M_{\odot}$, and based on the relation between the number of GCs and the virial mass of the host galaxy (Burkert & Forbes 2020), each UDG should then host, on average, 160 GCs. Using the average GC-LMXB luminosity function, this number of GCs, in turn, implies a combined GC-LMXB luminosity of about $9.0 \times 10^{39} \text{ erg s}^{-1}$ in the 0.5–7.0 keV band.

Using a sample of galaxies, Zhang et al. (2011) found that the X-ray luminosity for a large number of GC-LMXBs is less than $10^{38} \text{ erg s}^{-1}$, suggesting that most of them remain unresolved at the redshift of Coma based on the existing *XMM-Newton* observations. Therefore, we carried out the stacking analysis, as is done in Section 3.1, but this time in the 0.5–7.0 keV energy range, by co-adding the X-ray images and exposure maps associated with the individual UDGs. The source counts were extracted from a circular radius of 15 arcsec, and the background counts were extracted from a circular annulus with radii of 25–30 arcsec. As in Section 3.1, we did not obtain statistically significant X-ray emission from the source region, in agreement with that reported in Kovács et al. (2020). In the absence of significant emission, we computed the 2σ upper-limit flux by assuming that the X-ray emission from GC-LMXBs follows a power-law spectrum with a spectral index of 1.7. The 2σ upper-limit flux is $< 1.4 \times 10^{-16} \text{ erg s}^{-1} \text{ cm}^{-2}$, which places a 2σ upper limit of $< 1.8 \times 10^{38} \text{ erg s}^{-1}$ on the X-ray luminosity, at the redshift of the Coma cluster.

Despite that the upper limit on the X-ray luminosity is higher than

the 2σ upper-limit luminosity of $< 1.1 \times 10^{38} \text{ erg s}^{-1}$ reported in Kovács et al. (2020), it is about 50 times lower than that predicted for a UDG hosting a large number of GCs. This result indicates that the bulk of the UDG population in the Coma cluster does not host a large number of GCs, agreeing with that found in Kovács et al. (2020). This implies that significant fraction of the analysed UDGs are not the descendants of massive galaxies, but are genuine dwarf galaxies.

3.3 X-ray AGN identification

Since the mass of AGN correlates with the dark matter halo mass of the host galaxy (e.g. Bogdán & Goulding 2015), it is interesting to test whether the AGN occupation fraction of UDGs is comparable with that obtained for massive or dwarf galaxies. Kovács et al. (2020) reported only two UDGs out of 404 that have an off-centre X-ray source within a radius of 5 arcsec from the centre of the UDGs. Thus, they placed an upper limit of < 0.5 per cent on the occupation fraction of AGN in the Coma cluster UDGs. This value falls short of that reported for high-mass galaxies, but is more comparable with that found for dwarf galaxies (e.g. Miller et al. 2015; Kaviraj et al. 2019).

In this work, the AGN occupation fraction is computed using an approach similar to that presented in Kovács et al. (2020). We searched for AGN in the Coma cluster UDGs by cross-correlating the position of the analysed UDGs with the position of the point sources detected in the soft and broad bands. As in Kovács et al. (2020), we did not find any matches within a search radius of 2.5 arcsec from the centre of the UDGs. Increasing the search radius to 5 arcsec (corresponding to $2r_{\text{eff}}$ at the redshift of Coma), we detected three X-ray sources with detection significance $\sigma \geq 5$, in which their position matches with the position of the Coma’s UDGs. These galaxies are the UDG 317 ($r_{\text{eff}} = 2.7$ arcsec), UDG 432 ($r_{\text{eff}} = 1.9$ arcsec), and UDG 535 ($r_{\text{eff}} = 3.2$ arcsec), and the radii of the X-ray sources associated with them are 4.3, 5.1, and 7.3 arcsec, respectively. The offsets between these UDG coordinates and the detected point sources are, respectively, 2.9, 4.7, and 4.4 arcsec for the UDG 317, UDG 432, and UDG 535. In Fig. 4, we show the X-ray images of these UDGs and the detected point sources.

The identified point source within 5 arcsec from the UDG 317 centre (Fig. 4, left panel) is reported by Kovács et al. (2020). These authors also identified an X-ray source around UDG 412. However, we did not detect any X-ray sources around UDG 412 using the same searching radius. On the other hand, the identified X-ray sources around UDG 432 and UDG 535 (Fig. 4, middle and right panels) are not reported by Kovács et al. (2020). This is expected since the number of the studied UDGs here is greater, by a factor of about 2, than that studied in Kovács et al. (2020).

If we assume that these X-ray sources reside in the Coma cluster, their X-ray luminosity in the 0.5–7.0 energy band is $(8.1 \pm 0.8) \times 10^{38} \text{ erg s}^{-1}$, $(2.1 \pm 0.2) \times 10^{39} \text{ erg s}^{-1}$, and $(5.5 \pm 0.6) \times 10^{38} \text{ erg s}^{-1}$ for the UDG 317, UDG 432, and UDG 535, respectively. The luminosity of the identified point sources in the UDG 317 and UDG 535 is below $10^{39} \text{ erg s}^{-1}$, and their $B - R$ color indices are 0.91 and 0.93, respectively. Therefore, it is unlikely that these sources are high-mass X-ray binary (HMXB) or ultra-luminous X-ray (ULX) sources, but are more likely LMXBs (e.g. Gilfanov 2004; Kim & Fabbiano 2004). It is also possible that these sources are off-centre low-luminosity AGN. However, with a luminosity below $10^{39} \text{ erg s}^{-1}$, it is difficult to distinguish between the X-ray emission originating from an AGN and X-ray binaries (e.g. Lehmer et al. 2010; Baldassare et al. 2018). For the UDG 432, the luminosity of the identified point source exceeds

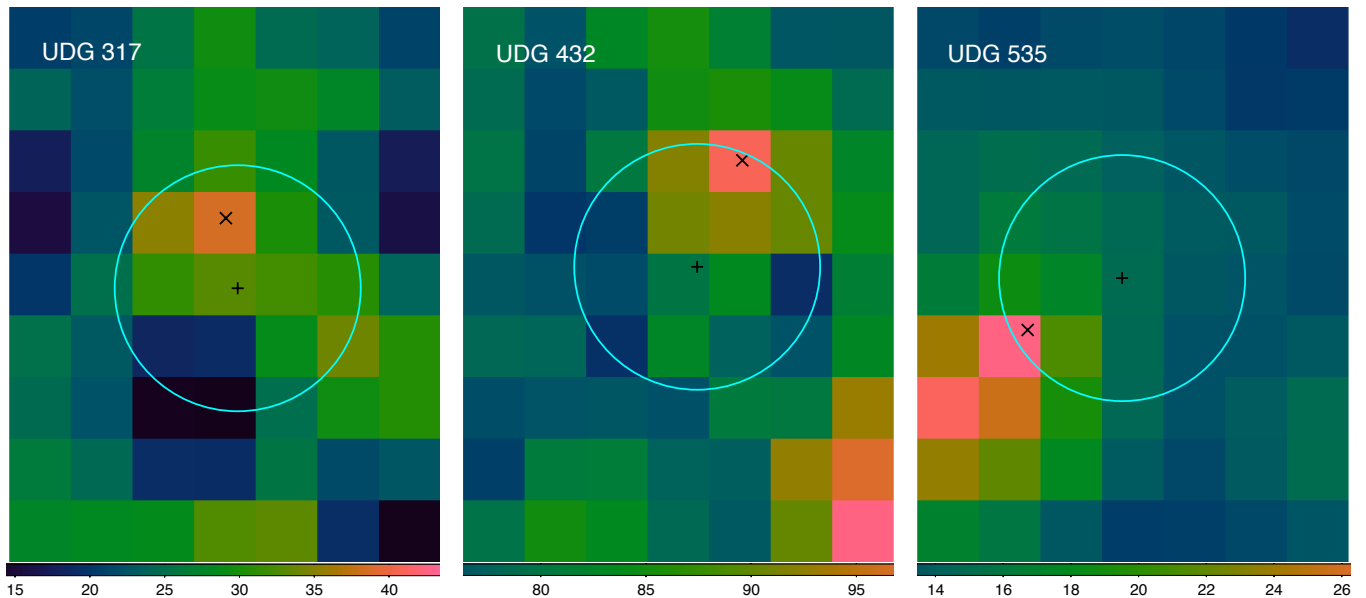


Figure 4. Exposure-corrected *XMM-Newton* images of UDG 317, UDG 432, and UDG 535 in the energy range 0.5–1.2 keV. The cyan circles have an angular radius of 5 arcsec and are centred on the UDG coordinates, shown as black plus marks. The coordinates of the detected point sources that lie within 5 arcsec from the UDG centres are shown as black cross marks.

10^{39} erg s^{-1} , indicating that it could either be a HMXB or ULX source. These X-ray sources, however, are typically associated with the ongoing star-formation activity (e.g. Mineo et al. 2012; Sazonov & Khabibullin 2017). It is found that the UDG 432 has a $B - R$ color index of 1.1 with no signature of $H\alpha$ emission (Koda et al. 2015), implying that this galaxy is not forming stars at the current epoch. This, in turn, suggests that the associated X-ray source is unlikely to be an HMXB or ULX, but is more likely an off-centre low-luminosity AGN, assuming that the UDG 432 resides in the Coma cluster and the X-ray source lies within the galaxy. However, there is still a possibility that the X-ray source is not a member of the Coma cluster, and is therefore a foreground or background object.

As the number of counts collected from the X-ray sources is very low, it is not possible to carry out precise spectroscopic measurements. However, as is done in Kovács et al. (2020), we computed a hardness ratio for these sources to determine their nature, using counts in the hard and soft energy bands. The hardness ratio is defined as $HR = (H - S)/(H + S)$, where H and S are the net counts in the hard and soft bands, respectively. The computed hardness ratio for the X-ray sources is 0.19, 0.22, and 0.20 for the UDG 317, UDG 432, and UDG 535, respectively. Assuming the X-ray spectrum of AGN follows a power law with a spectral slope lying in the range of the typically observed values ($\Gamma = 1.5 - 2.0$), the corresponding value for the AGN hardness ratio is then in the 0.04–0.23 range. This implies that the X-ray sources in the UDG 317, UDG 432, and UDG 535 might originate from AGN. A similar conclusion is obtained for the X-ray sources identified in Kovács et al. (2020).

With the current X-ray data, however, it is difficult to conclusively determine the true nature of the X-ray sources associated with these galaxies. Since we cannot confirm the nature of these sources, we set an upper limit on the AGN occupation fraction of UDGs. Based on the identification of three point sources within 5 arcsec from the UDG centre, which could be off-centre AGN, we obtain an upper limit of < 0.4 per cent on the AGN occupation fraction of the Coma

cluster UDGs. This is in agreement with that reported in Kovács et al. (2020).

4 DISCUSSION

4.1 UDG origin

We have investigated the formation scenarios of UDGs in the Coma cluster using two different approaches. The analysis procedure carried out in this work is similar to that used in Kovács et al. (2020). However, we have used a larger population of UDGs, which is almost twice the population of UDGs used in Kovács et al. (2020).

By utilizing *XMM-Newton* observations, we have probed the formation scenarios of UDGs in the Coma cluster through their hot gaseous halos and LMXBs residing in GCs. We did not obtain statistically significant X-ray emission from the hot gaseous halos or from GC-LMXBs in the stacked sample. In the absence of significant emission, we set a 2σ upper limit on measurements. Assuming an optically-thin plasma emission with a temperature of 0.2 keV and a metallicity of $0.2 Z_{\odot}$, we have obtained a 2σ upper limit of $< 1.2 \times 10^{38}$ erg s^{-1} on the X-ray luminosity of the hot gaseous halo, which is around 9 times lower than that derived for a galaxy residing in a massive dark matter halo. For GC-LMXBs, we have obtained a 2σ upper limit of $< 1.8 \times 10^{38}$ erg s^{-1} on the X-ray luminosity, which is around 50 lower than that derived for a galaxy hosting a large number of GCs. These results indicate that the average UDG population does not have a substantial amount of hot X-ray gas or a large number of GCs. Based on these results, we conclude that most UDGs in the Coma cluster are genuine dwarf galaxies. This conclusion agrees with that obtained for the Coma cluster UDGs studied in Kovács et al. (2020) using *Chandra* observations. It is also in agreement with the conclusion derived for a sample of isolated UDGs (Kovács et al. 2019).

However, we cannot rule out the possibility that some individual UDGs, or small sub-samples of them, may have different formation

pathways. It is possible that some UDGs are the result of processing by the large-scale dense environment, and formed either as extended, low-surface brightness galaxies or as small, low-mass galaxies (e.g. Gnedin 2003; Collins et al. 2013). It is also possible that some UDGs are the descendants of massive galaxies, but lost their gas at high redshift due to extreme feedback from ram-pressure stripping (e.g. Fujita 2004), supernovae (e.g. Agertz & Kravtsov 2016), and AGN activity (e.g. Moran et al. 2014). This, in turn, quenched the star formation in these systems, forming extended and low-surface brightness galaxies with massive dark matter halos.

Beasley et al. (2016) found that the UDG VCC 1287 in the Virgo cluster hosts a large GC population. Similar results were also reported for the UDGs Dragonfly 17 (Peng & Lim 2016), Dragonfly 44, and DF X1 (van Dokkum et al. 2017) in the Coma cluster. The number of GCs detected in these systems is significantly larger than that typically detected in dwarf galaxies (e.g. Georgiev et al. 2010). This large GC population around these galaxies supports the formation scenario, in which UDGs reside in massive dark matter halos. These results, however, do not contradict with our findings since we stacked a large number of UDGs, and we therefore probed their average properties. Besides, more recent studies (Lee et al. 2020; Bogdán 2020) have found that Dragonfly 44 and DF X1 do not host significant X-ray emission. Therefore, as for the bulk of the UDGs, the same conclusion can also be applied to these galaxies.

4.2 AGN occupation fraction

In addition to probing the formation scenarios, we have constrained the AGN occupation fraction of UDGs in the Coma cluster. As discussed in Section 3.3, we have identified three X-ray sources within a radius of 5 arcsec from the centre of the UDG 317, UDG 432, and UDG 535 (Fig. 4). Based on the current data, we cannot conclusively determine the redshift and nature of the X-ray sources associated with these UDGs. They could be off-centre AGN residing in the galaxies, foreground X-ray binaries, or background AGN.

However, if we assume that these UDGs reside in the Coma cluster and the identified X-ray sources are within the field of these galaxies, these sources are then likely off-center low-luminosity AGN. The offset between these UDG coordinates and the detected X-ray sources ranges between 2.9–4.7 arcsec, which corresponds to 1.4–2.3 kpc at the redshift of the Coma cluster. The presence of such offsets is likely in dwarf galaxies, and is in agreement with those reported in Kovács et al. (2020). These offsets are also in agreement with those offsets found in X-ray and radio surveys of AGN in dwarf galaxies (e.g. Mezcua et al. 2018; Reines et al. 2020). Furthermore, high-resolution cosmological simulations (e.g. Bellovary et al. 2019) predicted that about half of massive black holes in dwarf galaxies are not centrally located, but rather are locating at distances of a few kpc from the galaxy centre.

Based on the identification of three X-ray sources within 5 arcsec from the galaxy centre, which could be off-centre low-luminosity AGN, we have placed an upper limit of < 0.4 per cent on the occupation fraction of AGN in the Coma cluster UDGs. This upper limit agrees well with an upper limit of < 0.5 per cent on the AGN occupation fraction reported in Kovács et al. (2020). Our result is also consistent with an AGN occupation fraction of about 0.6 per cent reported for a sample of dwarf galaxies with stellar masses of $10^{8.5} < M_{\text{star}} < 10^{9.5} M_{\odot}$ utilizing data from the Sloan Digital Sky Survey (SDSS; Reines et al. 2013). However, our estimated value for the AGN occupation fraction falls significantly short of the values obtained for early-type galaxies in the AMUSE (AGN Multi-wavelength Survey of Early-type galaxies) survey (Miller & Bregman 2015). For

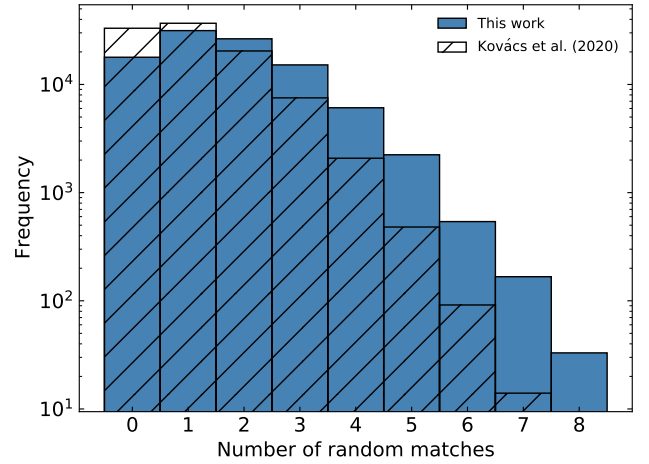


Figure 5. Number of random X-ray source-UDG matches within the *XMM-Newton* footprint of the Coma cluster for 779 randomly generated UDG coordinates using Monte Carlo simulations with 10^5 trials. We also show the result of Monte Carlo simulations from Kovács et al. (2020) (hatched histogram). The number of random matches ranges between 0–8, with about 60 per cent of them in the range of 1 to 2. The average number of random matches is 1.70, suggesting that two of the three identified X-ray sources, at least, are likely due to the result of random matches.

galaxies with $M_{\text{star}} < 10^{10} M_{\odot}$, these authors placed an lower limit of 20 per cent on the AGN occupation fraction, which exceeds the upper limit obtained for the UDGs in the Coma cluster by a factor of about 50. This difference in the AGN occupation fraction may be partially due to the higher sensitivity of the AMUSE survey, which allows to detect fainter X-ray sources.

It is possible that the X-ray sources associated with the UDG 317, UDG 432, and UDG 535 are not AGN in these galaxies, but are foreground or background objects. Therefore, their existence within a radius of 5 arcsec from the centre of the UDGs is due to random matches. To quantify the likelihood of random matches, we performed Monte Carlo simulations, as is done in Kovács et al. (2020). After excluding the central 4 arcmin region, we generated 779 random coordinates within the footprint of the *XMM-Newton* observations for the Coma cluster. We then searched for coincident matches within 5 arcsec between the position of the randomly generated coordinates and the position of the detected X-ray sources in the soft and broad bands. We repeated this process 10^5 times, and the number of random matches was recorded at each time.

In Fig. 5, we present a histogram showing the result of Monte Carlo simulations. The number of random X-ray source-UDG matches ranges between 0–8, with about 60 per cent of them in the range of 1 to 2. The average number of random matches is 1.70, which corresponds to an average AGN occupation fraction of 0.22 per cent. These results suggest that two of the three identified X-ray sources, at least, are likely due to the result of random matches.

To set further constraint on the nature of the identified X-ray sources, we inspected the regions around the UDG 317, UDG 432, and UDG 535 in the optical band using Digitized Sky Survey (DSS) and Subaru images. We identified an optical source within a radius of 5 arcsec from the UDG 317 centre, matching the position of the X-ray source. However, no optical counterparts were detected for the X-ray sources associated with the UDG 432 and UDG 535. Also, we checked images of these UDGs in FIR and other wave bands, but we did not find any significant sources in the field of

these galaxies. Using the Subaru images, Kovács et al. (2020) also identified an optical counterpart for the X-ray source associated with the UDG 317. The detection of an optical counterpart implies that the X-ray source associated with the UDG 317 is an off-centre AGN. However, this detection does not constrain whether the detected AGN is residing in the Coma cluster or not. Therefore, we cannot rule out the possibility that it could be a background or foreground object.

5 CONCLUSIONS

In this work, we have probed the formation scenarios and AGN occupation fraction of 779 UDG candidates in the nearby Coma cluster, following an X-ray analysis similar to that presented in Kovács et al. (2020). The formation scenarios of UDGs were probed by constraining their dark matter halo mass using two approaches. Since the dark matter halo mass correlates with the X-ray luminosity, we have measured the X-ray luminosity of hot gas and GC-LMXB by stacking the X-ray photons of a large sample of UDGs. We did not detect statistically significant emission from hot gas or from LMXBs residing in GCs. In the absence of significant detection, we have placed 2σ upper limits of $< 1.2 \times 10^{38} \text{ erg s}^{-1}$ and $< 1.8 \times 10^{38} \text{ erg s}^{-1}$ on the X-ray luminosity expected from hot gas and GC-LMXBs, respectively. The upper limits fall significantly short of the X-ray luminosities expected from UDGs residing in massive dark matter halos and hosting significant population of GCs. These results suggest that significant fraction of UDG candidates in the Coma cluster reside in low-mass dark matter halos, implying that they are puffed-up dwarf galaxies. This conclusion agrees with that obtained for 404 UDGs in the Coma cluster using *Chandra* observations (Kovács et al. 2020). It is also in agreement with the conclusion derived for a sample of isolated UDGs (Kovács et al. 2019).

Moreover, we have constrained the AGN occupation fraction of UDGs by cross-correlating the position of UDGs with the identified X-ray sources in the Coma cluster. We have identified three X-ray sources that could be AGN at distances of 2.9, 4.7, and 4.4 arcsec from the centre of the UDG 317, UDG 432, and UDG 535, respectively. Since spectroscopic measurements are not available for them, we cannot conclusively determine the true nature of these sources. Also, Monte Carlo simulations indicate that two of these sources are likely due to spatial coincidence. Based on these results, we have placed an upper limit of < 0.4 per cent on the AGN occupation fraction of UDGs in the Coma cluster, which is comparable with that found for dwarf galaxies.

Deep observations with the current X-ray observatories are required to carry out precise spectroscopic measurements and establish whether the UDGs and associated X-ray sources are residing in the Coma cluster. However, a complete understanding of the origin and evolutionary picture of UDGs can only be achieved with upcoming high-resolution spectral X-ray observations such as *Athena* (Barcons et al. 2017), and proposed concepts such as *Lynx* (Gaskin et al. 2019) and *AXIS* (Mushotzky et al. 2019).

ACKNOWLEDGEMENTS

We thank the referee for their helpful report. MSM and SAW acknowledge support from the NASA *XMM-Newton* grant 19-XMMN18-0030. Based on observations obtained with *XMM-Newton*, an ESA science mission with instruments and contributions directly funded by ESA Member States and NASA.

DATA AVAILABILITY

The *XMM-Newton* Science Archive (XSA) stores the archival data used in this paper, from which the data are publicly available for download. The *XMM* data were processed using the *XMM-Newton* Science Analysis System (SAS). The software packages HEASOFT and XSPEC were used, and these can be downloaded from the High Energy Astrophysics Science Archive Research Centre (HEASARC) software web-page. Analysis and figures were produced using PYTHON version 3.7.

REFERENCES

- Abraham R. G., van Dokkum P. G., 2014, *PASP*, 126, 55
 Agertz O., Kravtsov A. V., 2016, *ApJ*, 824, 79
 Amorisco N. C., Loeb A., 2016, *MNRAS*, 459, L51
 Angelini L., Loewenstein M., Mushotzky R. F., 2001, *ApJ*, 557, L35
 Babyk I. V., McNamara B., Nulsen P., Hogan M., Vantghem A., Russell H., Pulido F., Edge A., 2018, *ApJ*, 857, 32
 Baldassare V. F., Geha M., Greene J., 2018, *ApJ*, 868, 152
 Barcons X., et al., 2017, *Astron. Nachr.*, 338, 153
 Beasley M. A., Romanowsky A. J., Pota V., Navarro I. M., Delgado D. M., Neyer F., Deich A. L., 2016, *ApJ*, 819, L20
 Bellovary J. M., Cleary C. E., Munshi F., Tremmel M., Christensen C. R., Brooks A., Quinn T. R., 2019, *MNRAS*, 482, 2913
 Bogdán Á., 2020, *ApJ*, 901, L30
 Bogdán Á., Goulding A. D., 2015, *ApJ*, 800, 124
 Burkert A., Forbes D. A., 2020, *AJ*, 159, 56
 Collins M. L., et al., 2013, *ApJ*, 768, 172
 Fujita Y., 2004, *PASJ*, 56, 29
 Gaskin J. A., et al., 2019, *J. Astron. Telesc. Instrum. Syst.*, 5, 021001
 Georgiev I. Y., Puzia T. H., Goudfrooij P., Hilker M., 2010, *MNRAS*, 406, 1967
 Gilfanov M., 2004, *MNRAS*, 349, 146
 Gnedin O. Y., 2003, *ApJ*, 589, 752
 Goulding A. D., et al., 2016, *ApJ*, 826, 167
 Impey C., Bothun G., Malin D., 1988, *ApJ*, 330, 634
 Irwin J. A., Athey A. E., Bregman J. N., 2003, *ApJ*, 587, 356
 Jordán A., et al., 2007, *ApJ*, 671, L117
 Kaviraj S., Martin G., Silk J., 2019, *MNRAS*, 489, L12
 Kim D.-W., Fabbiano G., 2004, *ApJ*, 611, 846
 Kim D.-W., Fabbiano G., 2013, *ApJ*, 776, 116
 Kim E., Kim D.-W., Fabbiano G., Lee M. G., Park H. S., Geisler D., Dirsch B., 2006, *ApJ*, 647, 276
 Koda J., Yagi M., Yamanoi H., Komiyama Y., 2015, *ApJ*, 807, L2
 Kovács O. E., Bogdán Á., Canning R. E., 2019, *ApJ*, 879, L12
 Kovács O. E., Bogdán Á., Canning R. E. A., 2020, *ApJ*, 898, 164
 Lakhchaura K., et al., 2018, *MNRAS*, 481, 4472
 Lee C. H., Hodges-Kluck E., Gallo E., 2020, *MNRAS*, 497, 2759
 Lehmer B., Alexander D., Bauer F., Brandt W. N., Goulding A., Jenkins L., Ptak A., Roberts T., 2010, *ApJ*, 724, 559
 Mezcua M., Civano F., Marchesi S., Suh H., Fabbiano G., Volonteri M., 2018, *MNRAS*, 478, 2576
 Mihos J. C., et al., 2015, *ApJ*, 809, L21
 Miller M. J., Bregman J. N., 2015, *ApJ*, 800, 14
 Miller B. P., Gallo E., Greene J. E., Kelly B. C., Treu T., Woo J.-H., Baldassare V., 2015, *ApJ*, 799, 98
 Mineo S., Gilfanov M., Sunyaev R., 2012, *MNRAS*, 419, 2095
 Minniti D., Rejkuba M., Funes J. G., Akiyama S., et al., 2004, *ApJ*, 600, 716
 Mirakhor M. S., Walker S. A., 2020a, *MNRAS*, 497, 3204
 Mirakhor M. S., Walker S. A., 2020b, *MNRAS*, 497, 3943
 Moran E. C., Shahinyan K., Sugarman H. R., Vélez D. O., Eracleous M., 2014, *ApJ*, 148, 136
 Muñoz R. P., et al., 2015, *ApJ*, 813, L15
 Mushotzky R., et al., 2019, *Bull. Am. Astron. Soc.*, 51, 107
 Peng E. W., Lim S., 2016, *ApJ*, 822, L31

- Piconcelli E., Jimenez-Bailón E., Guainazzi M., Schartel N., Rodríguez-Pascual P., Santos-Lleó M., 2005, *A&A*, 432, 15
- Reines A. E., Greene J. E., Geha M., 2013, *ApJ*, 775, 116
- Reines A. E., Condon J. J., Darling J., Greene J. E., 2020, *ApJ*, 888, 36
- Sarazin C. L., Irwin J. A., Bregman J. N., 2000, *ApJ*, 544, L101
- Sazonov S., Khabibullin I., 2017, *MNRAS*, 466, 1019
- Sivakoff G. R., et al., 2007, *ApJ*, 660, 1246
- Yagi M., Koda J., Komiyama Y., Yamanoi H., 2016, *ApJS*, 225, 11
- Zhang Z., et al., 2011, *A&A*, 533, A33
- van Dokkum P. G., Abraham R., Merritt A., Zhang J., Geha M., Conroy C., 2015, *ApJ*, 798, L45
- van Dokkum P., et al., 2016, *ApJ*, 828, L6
- van Dokkum P., et al., 2017, *ApJ*, 844, L11

APPENDIX A: *XMM-NEWTON* OBSERVATIONS OF THE COMA CLUSTER

This paper has been typeset from a $\text{\TeX}/\text{\LaTeX}$ file prepared by the author.

Table A1. *XMM–Newton* observations of Coma

Observation	Obs. ID	Obs. Date	RA (J2000)	Dec. (J2000)	Exposure (ks)
Outskirts1	0841680101	07 Jul 2019	12 55 25.59	+27 47 01.6	23.0
Outskirts2	0841680201	07 Jul 2019	12 55 38.07	+28 17 43.1	23.0
Background1	0841681101	12 Jul 2019	12 53 31.92	+28 29 54.4	29.5
Outskirts3	0841680301	11 Jul 2019	12 57 03.20	+28 41 26.5	26.0
Outskirts4	0841680401	13 Jul 2019	12 59 11.76	+28 52 56.4	23.0
Outskirts5	0841680501	13 Jul 2019	13 01 27.90	+28 51 36.7	23.0
Outskirts6	0841680601	17 Jul 2019	13 03 15.79	+28 32 54.7	23.0
Background2	0841681201	29 Dec 2019	13 05 10.70	+28 53 08.8	23.0
Outskirts7	0841680701	16 Jul 2019	13 04 03.83	+28 04 45.1	26.4
Outskirts8	0841680801	17 Jul 2019	13 03 56.84	+27 35 23.5	34.4
Outskirts9	0841680901	06 Dec 2019	13 02 49.88	+27 11 18.6	30.8
Outskirts10	0800580101	23 Dec 2017	13 00 57.97	+26 58 35.3	80.4
Outskirts10	0800580201	04 Jan 2018	13 00 57.97	+26 58 35.3	87.0
Outskirts11	0403150301	17 Jun 2006	12 57 40.75	+26 56 13.6	56.0
Outskirts11	0403150401	21 Jun 2006	12 57 40.75	+26 56 13.6	64.4
Outskirts12	0058940701	10 Jun 2003	12 55 24.99	+27 13 46.0	22.6
Inside1	0124710501	29 May 2000	12 59 27.49	+27 46 53.0	29.9
Inside2	0124711401	29 May 2000	12 59 46.71	+27 56 60.0	34.6
Inside3	0124711601	11 Jun 2000	12 57 42.51	+27 43 38.0	87.9
Inside4	0124710201	11 Jun 2000	12 57 42.51	+27 43 38.0	41.5
Inside5	0124710901	11 Jun 2000	13 00 32.68	+27 56 59.0	31.2
Inside6	0124710601	12 Jun 2000	12 58 50.01	+27 58 52.0	31.8
Inside7	0124710101	21 Jun 2000	12 56 47.68	+27 24 07.0	41.5
Inside8	0124710401	23 Jun 2000	13 00 04.60	+27 31 24.0	52.8
Inside9	0124711101	24 Jun 2000	12 58 36.51	+28 23 56.0	40.0
Inside10	0124710701	24 Jun 2000	12 57 27.68	+28 08 41.0	27.2
Inside11	0124710301	27 Jun 2000	12 58 32.19	+27 24 12.0	28.6
Inside12	0124712201	09 Dec 2000	12 57 42.51	+27 43 38.0	27.6
Inside13	0124712001	10 Dec 2000	12 58 50.01	+27 58 52.0	22.8
Inside14	0124712101	10 Dec 2000	12 57 27.68	+28 08 41.0	28.1
Inside15	0124710801	10 Dec 2000	13 01 25.60	+27 43 53.0	29.8
Inside16	0153750101	04 Dec 2001	12 59 46.71	+27 56 60.0	25.8
Inside17	0124712401	05 Jun 2002	13 01 50.19	+28 09 28.0	27.6
Inside18	0124712501	07 Jun 2002	13 00 36.50	+28 25 15.0	28.7
Inside19	0204040101	06 Jun 2004	13 00 22.21	+28 24 03.0	101.9
Inside20	0204040201	18 Jun 2004	13 00 22.21	+28 24 03.0	108.3
Inside21	0204040301	12 Jul 2004	13 00 22.21	+28 24 03.0	104.2
Inside22	0300530701	06 Jun 2005	12 59 36.92	+27 58 14.8	25.5
Inside23	0300530601	07 Jun 2005	12 59 35.41	+27 56 33.3	25.7
Inside24	0300530501	08 Jun 2005	12 59 39.73	+27 55 12.0	25.5
Inside25	0300530401	09 Jun 2005	12 59 46.67	+27 55 12.0	27.5
Inside26	0300530301	11 Jun 2005	12 59 51.00	+27 56 33.3	31.0
Inside27	0300530201	17 Jun 2005	12 59 49.45	+27 58 14.8	27.5
Inside28	0300530101	18 Jun 2005	12 59 43.18	+27 58 59.8	25.5
Inside29	0304320301	27 Jun 2005	13 00 22.21	+28 24 03.0	55.9
Inside30	0304320201	28 Jun 2005	13 00 22.21	+28 24 03.0	80.8
Inside31	0304320801	06 Jun 2006	13 00 22.21	+28 24 03.0	63.8
Inside32	0403150201	11 Jun 2006	12 57 42.51	+27 19 09.7	55.2
Inside33	0403150101	14 Jun 2006	12 57 42.51	+27 19 09.7	54.4
Inside34	0652310701	16 Jun 2010	12 57 24.29	+27 29 52.0	21.8
Inside35	0652310201	18 Jun 2010	12 57 24.29	+27 29 52.0	22.3
Inside36	0652310301	20 Jun 2010	12 57 24.29	+27 29 52.0	19.4
Inside37	0652310401	24 Jun 2010	12 57 24.29	+27 29 52.0	23.9
Inside38	0652310501	04 Jul 2010	12 57 24.29	+27 29 52.0	22.9
Inside39	0652310601	06 Jul 2010	12 57 24.29	+27 29 52.0	20.8
Inside40	0652310801	03 Dec 2010	12 57 24.29	+27 29 52.0	16.9
Inside41	0652310901	05 Dec 2010	12 57 24.29	+27 29 52.0	16.9
Inside42	0652311001	11 Dec 2010	12 57 24.29	+27 29 52.0	16.4
Inside43	0691610201	02 Jun 2012	12 57 24.65	+27 29 42.7	37.9
Inside44	0691610301	04 Jun 2012	12 57 24.65	+27 29 42.7	35.9
Inside45	0851180501	30 May 2019	13 02 00.14	+27 46 57.8	48.4